Science Press

ARTICLE

# Performance of Oxygen-Carbon Co-cementation Coating on Titanium Alloy

Ji Shouchang[1,2,3],    Li Jinglong[1,2],    Wang Shaopeng[3],    Yang Haiyu[3],    Chang Chenyang[3]

[1] State Key Laboratory of Solidification Processing, Northwestern Polytechnical University, Xi`an 710072, China; [2] Shaanxi Key Laboratory of Friction Welding Technologies, Northwestern Polytechnical University, Xi`an 710072, China; [3] Northwest Institute for Nonferrous Metal Research, Xi`an 710016, China

**Abstract:** The Ti6Al4V alloy specimens were planished, polished, cleaned by ethyl-alcohol with ultrasonic, and dried. Then, the treated specimens were put into a special equipment for oxygen-carbon co-cementation. The X-ray diffractometer (XRD), scanning electron microscope (SEM), energy disperse spectroscope (EDS), HV hardness tester, and universal material testing machine were used to analyze the phase, microstructure, composition, hardness, frictional wear, and mechanical properties of the co-cemented layer. XRD results show that TiC and $TiO_x$ phases appear in the co-cemented layer. The microstructure of the original Ti6Al4V alloy specimen is changed by the oxygen-carbon co-cementation. The microstructure of the co-cemented layer is obviously different from that of Ti6Al4V alloy specimens after carburization treatment, oxygen permeation treatment, and treatment under $CO_2$ atmosphere. EDS results show that the content of C and O elements changes gradually. The surface hardness of the co-cemented layer is 3.8 times higher than that of the substrate, and the hardness of the co-cemented layer also changes gradually. The oxygen-carbon co-cementation changes the adhesive wear and friction state of the original specimen. Only slight friction trace occurs on the surface of the co-cemented specimen and no wear appears. The wear amount of the co-cemented specimen is 3.5% of that of the original specimen, and the friction coefficient is about 30% of that of the original specimen. In the tensile fracture process, the outer surface of the co-cemented specimen peels off to a certain extent, and the surface is covered by cracks, resulting in the slightly decreased strength of the specimen. The elongation and the reduction of area are comparable to those of the original specimen. After oxygen-carbon co-cementation of Ti6Al4V alloy, the surface hardness of the specimen is improved, the wear rate and friction coefficient are reduced, and the mechanical properties of the specimens basically remain.

**Key words:** titanium; oxygen-carbon; co-cementation; hardness; wear resistance; mechanical property

Titanium and titanium alloys, as one of the most promising structural materials, have been widely used in many industry fields, especially in aerospace, aviation, and petrochemical fields, because they have superior comprehensive properties, such as low density, excellent corrosion and erosion resistance, and good high-temperature behavior. However, the titanium and titanium alloys have poor abrasive wear resistance and low hardness. The hardness of pure titanium is 1470~1960 MPa, and that of the common titanium alloys is below 3920 MPa. Therefore, it is necessary to prepare a coating on the surface of titanium and its alloys for wear resistance, especially under heavy loading conditions[1-3].

The treatment of titanium alloys has been extensively studied. The carburization and nitridation treatments can easily increase the hardness of the titanium alloys. Particularly, the hydrogen-free carbonization treatment is a simple and efficient method to improve the surface properties of titanium alloys[3-6], and it can inhibit the hydrogen permeation. As a result, the hydrogen brittleness of titanium alloys can be fundamentally solved[5-7]. The hardness of the titanium alloy after hydrogen-free carburization is more than 98 GPa. However, the white and dense TiC layer can be formed. Because the carbon has a very low solid solubility in titanium, there is no significant carbon diffusion zone beneath

the TiC layer, indicating that the layer hinders the further diffusion of carbon towards the titanium substrate. Therefore, it is difficult to obtain a relatively thick carburized coating[3-7].

The atomic radii of the related elements are arranged in order as C>N>O, indicating that O is more attractive to Ti. Therefore, the oxygen has obvious solid-solubility strengthening effect, i.e., the oxygen permeation treatment on the titanium alloy surface can obtain an oxygen-solubility strengthening coating. In addition, the oxygenation and oxygen diffusion (OD) occur more easily at high temperatures than the carburization does on titanium alloys. It is known that OD and thermal oxidization (TO) are commonly used methods to improve the hardness of titanium alloys. However, the enhanced hardness is still low of 5880~6860 MPa[8-17].

During the carbonization process, the simultaneous oxygen permeation can break the dense titanium carbide layer on the titanium surface, and form a hydrogen-free oxygen-carbon co-cementation layer on the titanium surface, resulting in a thick carburization layer with high hardness and without hydrogen embrittlement[18]. Under the condition of carbon atmosphere, the oxygen-carbon co-cemented layer can be prepared on the titanium surface by introducing $CO_2$ into the system at a specific temperature[18-21].

The oxidation behavior of titanium at different temperatures in the $CO_2$ atmosphere or Ar-$CO_2$ atmosphere without carbon source has been widely studied. Usually, the double-layer structures with the rutile ($TiO_2$) and porous microstructures can be obtained, and these layers are very thick with perio-dically multiple patterns. With prolonging the oxidation time or increasing the oxidation temperature, these porous oxide layers constantly blister, crack, and even peel off, then a new porous oxide layer is formed, and the break-formation cycle is continuously repeated. Under these porous oxide layers, there is an oxygen-rich zone or oxygen-permeated zone, which varies with treatment temperature, duration, flow rate of $CO_2$, and gas ratio. The oxidation process is caused either by the outward diffusion of titanium or the inward diffusion of oxygen through the oxygen-rich zone or the oxygen-permeated zone. When the external layers peel off, the internal layers become external layers, and the oxygen-rich zone or the oxygen-permeated zone becomes the internal layer. When the oxidation temperature is low or the oxidation duration is short, these layers maintain their status or peel off slowly[21,22].

Generally, the titanium can be hardened by the single carburization or the oxygen permeation method. Nowadays, the research on the oxygen-carbon co-cementation is rarely reported, and few patents are related to this field[18-21]. In this research, the oxygen-carbon co-cementation was conducted on the surface of Ti6Al4V titanium alloy. The phase and structure of co-cemented layer were studied, and the effect of oxygen-carbon co-cemented layer on the wear resistance and mechanical properties of the titanium alloys were discussed[22-27].

# 1  Experiment

Ti6Al4V alloy was used as the substrate (Western

Superconducting Technologies Co., Ltd), and its composition is shown in Table 1.

The Ti6Al4V alloy specimens were planished, polished, cleaned by ethyl-alcohol with ultrasonic, and dried. Then, the specimens were put into a vacuum furnace, as shown in Fig.1[23]. The vacuum degree was $5\times10^{-3}$ Pa. The furnace was heated to the set temperature, and then $CO_2$ was input into the vacuum furnace to adjust the pressure. Then the oxygen-carbon co-cementation experiments were conducted, according to the procedures in Ref.[23].

The specimens were cut by the WEDM equipment for cross-sectional observation. Afterwards, the specimens were polished, cleaned, and dried. The phase structure of the coating was analyzed by the Rigaku D/max-2200pc X-ray diffractometer (XRD, Cu-Kα, 40 kV, 40 mA, 20°~80°). The morphology of the coating was observed by JSM6460 scanning electron microscope (SEM). The composition analysis was conducted by the Oxford X-sight energy disperse spectroscope (EDS). The hardness was measured by HX-1000 equipment (Shanghai Taiming Optical Instrument Co., Ltd) with the load of 1.98 N and time of 15 s. The ball disk friction test was conducted by the MS-T3000 friction and wear tester (Lanzhou Institute of Chemical Physics, Chinese Academy of Sciences) with GCr15 ball as the friction pair under the condition of dry friction, load of 50 g, speed of 1300 r/min, rotation diameter of 15 mm, and time of 30 min. The wear loss was measured by the electronic balance with the accuracy of 0.0001 g. The mechanical properties were measured by the universal material testing machine (Instron 5982). For comparison, the abovementioned properties of original Ti6Al4V alloy and oxygen-carbon co-cemented alloy were all measured and analyzed.

# 2  Results and Discussion

## 2.1  Phase structure

XRD pattern of the co-cemented coating is shown in Fig.2, which demonstrates the existence of TiC, $TiO_2$ rutile, and $Ti_2O$ (hexagonal structure). The input $CO_2$ can react with the graphite ($CO_2$+C→CO). Then the CO reacts with the Ti6Al4V

**Table 1  Chemical composition of Ti6A14V alloy (wt%)**

| Al | V | Fe | C | N | H | Ti |
|---|---|---|---|---|---|---|
| 6.20 | 4.22 | 0.05 | 0.15 | 0.013 | 0.003 | Bal. |


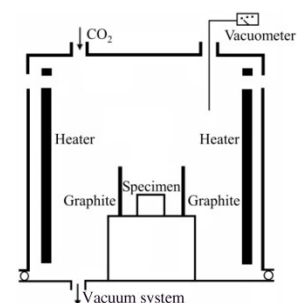
Fig.1  Schematic diagram of vacuum furnace for oxygen-carbon co-cementation[23]

Fig.2 XRD pattern of oxygen-carbon co-cemented coating on Ti6Al4V alloy



Fig.3 Surface morphology and EDS analysis results of oxygen-carbon co-cemented coating

substrate ($Ti+CO \rightarrow TiC+TiO_x$). As a result, TiC and $TiO_x$ occur on the surface of the co-cemented alloy.

**2.2 Morphology**

2.2.1 Surface morphology of oxygen-carbon co-cemented coating

The surface morphology and EDS analysis results of oxygen-carbon co-cemented coating is shown in Fig.3. It can be seen that coating surface is dark and dense without defects, such as crack, peeling, or bubble. When the specimen surface is ground, the coating color becomes light gradually, i.e., the denser the surface morphology, the darker the surface color and the smaller the surface roughness: black (about 15 μm)→ black-red (about 35 μm)→black-gray (about 60 μm)→light black (about 80 μm)→white (about 100 μm). According to EDS analysis of the specimen surface, in addition to Ti, Al, and V elements, C and O elements can also be detected.

2.2.2 Cross-section morphology of oxygen-carbon co-cemented coating

Fig. 4 shows SEM cross-section morphologies of the oxygen-carbon co-cemented coating. It can be found that the oxygen-carbon co-cementation can change the microstructure of Ti6Al4V alloy. The morphologies of titanium alloys after hydrogen-free carburization treatment, oxygen permeation treatment, or the treatment under $CO_2$ atmosphere usually present the characteristics of fine equiaxed crystal, porous solution layer, or porous multi-layer structures, which are quite different from the morphologies of oxygen-carbon co-
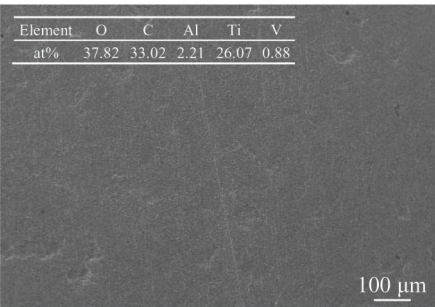
cemented coating. The oxygen-carbon co-cemented layer does not possess the white dense TiC layer of the carbonized coating[3], indicating that the oxygen permeation damages the dense layer structure, which is conducive to the carbon diffusion into the substrate. An oval morphology appears on the coating, because the coating peels off to some extent during the high-speed grinding process, which is attributed to the brittleness of the outer surface area.

EDS analysis results of the fracture of the co-cemented coating are shown in Fig.5. It can be seen that the C element appears at all five points; O element only appears at Point 1, 2, and 3, which is about 30 μm away from the surface. The diffusion rate of carbon in titanium alloys varies from $2 \times 10^{-9}$ $cm^2/s$ to $13 \times 10^{-9}$ $cm^2/s$ at the temperature of 1009~1108 K; the diffusion rate of oxygen in titanium alloys is $0.011 \times 10^{-9}$ $cm^2/s$ at 1023 K. Thus, the carbon diffuses much more rapidly than the oxygen does in titanium alloys[23]. With increasing the depth, the carbon content is decreased, because the carburization occurs through the diffusion. According to the Ti-C phase diagram[3], TiC phase can increase the hardness of Ti-based alloys. At Point 4 and 5, the carbon content is much lower than that at other points. Because Ti6Al4V alloy is the $\alpha+\beta$ binary alloy, the carbon solubility is 2.407 12at%~ 2.481 85at%, which is obtained by the formulae, as follows:

$$\lg x = 1.74 - 1800/T \qquad (873\sim1193 \text{ K}) \qquad (1)$$

$$\lg x = 1.4 - 2100/T \qquad (1193\sim1913 \text{ K}) \qquad (2)$$

where $x$ is the solubility of carbon in titanium (at%); $T$ is temperature (K).

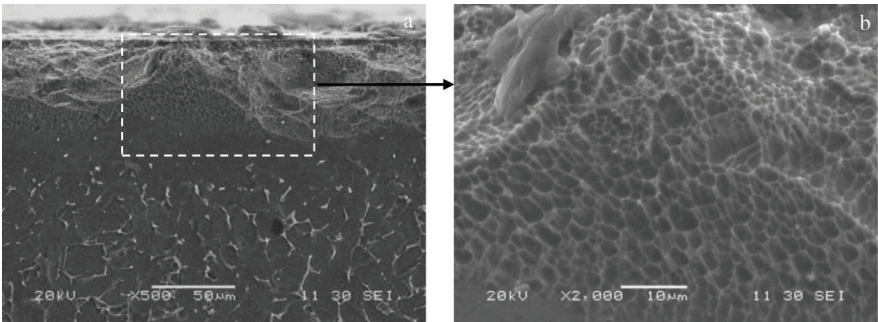The carbon content at Point 4 and 5 is 10.26at% and



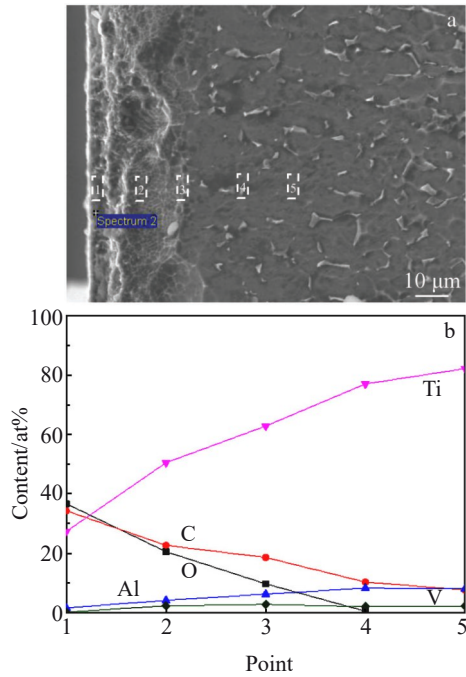Fig.4 SEM cross-section morphologies of oxygen-carbon co-cemented coating

Fig.5    SEM morphology (a) and EDS analysis results (b) of oxygen-carbon co-cemented coating

7.60at%, respectively, which is higher than the solubility of carbon in Ti6Al4V alloy. This phenomenon indicates that only a little carbon permeates the Ti6Al4V alloy substrate, i.e., this layer is only the effect layer of carburization, not a real carburization layer, which is different from the substrate.

## 2.3  Hardness

Fig. 6 shows the hardness results of co-cemented coating. The hardness increases sharply after the oxygen-carbon co-cementation and the surface hardness is 13 014 MPa, which is 3.8 times higher than that of the substrate (about 3430 MPa), and is also higher than that of the hydrogen-free carbonized coating (10 290 MPa)[5]. The depth of the hardened layer is about 200 μm, the hardness is decreased gradually with increasing the depth. This is because with increasing the depth, the carbon content is decreased, and thereby the TiC and $TiO_x$ hardened phases are decreased.
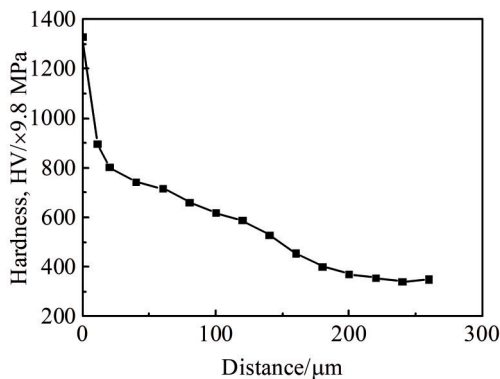


Fig.6    Hardness of oxygen-carbon co-cemented Ti6Al4V alloy

## 2.4  Wear resistance

### 2.4.1    Wear rate

The specimens were weighed before and after wear tests to determine the wear rates, as shown in Fig.7. The wear rate of the original Ti6Al4V alloy specimen is 0.1213 $g·h^{-1}$. After the oxygen-carbon co-cementation treatment, the wear rate is 0.0042 $g·h^{-1}$. The wear rate of the co-cemented specimen is only about 3.5% of that of the original specimen, demonstrating that the oxygen-carbon co-cementation can decrease the wear rate and improve the wear resistance of the alloys.

### 2.4.2    Friction coefficient

Fig. 8 shows the relationships between the friction coefficient and the friction distance of the Ti6Al4V alloys with and without oxygen-carbon co-cemented coating. Both the two curves enter the normal and stable wear stage after a short friction process. Afterwards, the friction coefficient of Ti6Al4V alloy is maintained at about 0.88, because the dynamic equilibrium occurs with the formation of wear scars and the increasing spilling[12], which leads to a steady friction coefficient. While the friction coefficient of co-cemented specimen increases firstly and then becomes stable at 0.27, which is about 30% of that of the original specimen. It is concluded that the wear resistance of Ti6Al4V alloy is greatly improved after the oxygen-carbon co-cementation.
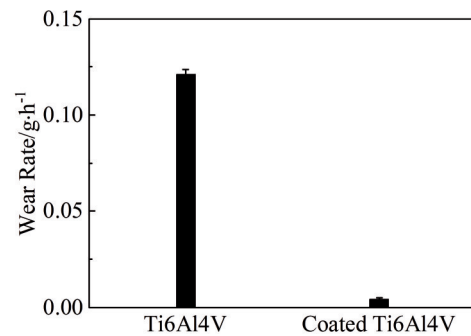


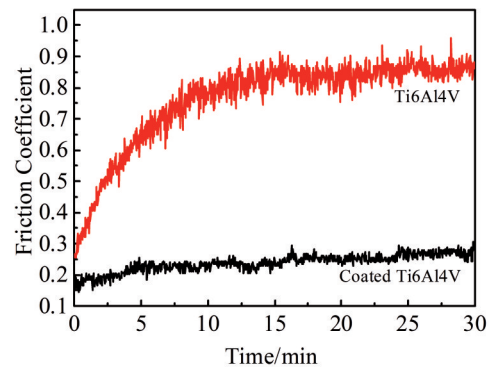Fig.7    Wear rate of Ti6Al4V alloys with and without oxygen-carbon co-cemented coating



Fig.8    Friction coefficients of Ti6Al4V alloys with and without oxygen-carbon co-cemented coating

### 2.4.3　Wear morphology

The wear morphologies and EDS analysis results of the Ti6Al4V alloy specimens with and without the oxygen-carbon co-cemented coating after sliding for 30 min (1838 m) are shown in Fig. 9. For the original Ti6Al4V alloy, the width of wear scar is 849.3 μm, and the furrows, wear particles, and adhesive belts appear. For the Ti6Al4V alloy with oxygen-carbon co-cemented coating, only the slight friction trace (87.2 μm) can be observed, no wear morphology occurs, and the trace width is only 10% of that of the original alloy. All these phenomena demonstrate that the oxygen-carbon co-cementation can improve the wear resistance of the alloy.

EDS results of wear particles in the original Ti6Al4V alloy in Fig. 9a show that the O element exists in the particles, which indicates that the oxidation occurs and the hardened particles are generated. The oxide particles are the hardened phase, which accelerate the abrasive wear against the original Ti6Al4V alloy substrate. As a result, the furrows occur on the wear surface with the wear process proceeding.

After the oxygen-carbon co-cementation, TiC and TiO$_x$ are generated on the coating surface, and their hardness is 13 014 MPa. The increased hardness corresponds to the improvement of wear resistance. The high hardness improves the plastic deformation resistance of alloy and reduces the viscosity. Besides, no adhesives remain on the alloy surface, inferring that the abrasive wear changes after the oxygen-carbon co-cementation.

### 2.5　Mechanical properties

#### 2.5.1　Tensile properties

Fig. 10 shows the tensile properties of the original Ti6Al4V alloy specimen (Original) and the co-cemented Ti6Al4V alloy specimen (Ti-C-O). In addition, the national standard tensile properties (GB) are also presented in Fig. 10 for comparison. It can be seen that compared with those of the Original specimen, the tensile strength and the specified non-proportional extension strength of Ti-C-O specimen are decreased by 4.2% and 2.3%, respectively. After the hydrogen-free carburization on the titanium surface, the tensile strength and the specified non-proportional extension strength of Ti6Al4V alloy both reduce by 5%, compared with those of the Original specimen. Thus, the oxygen-carbon co-cementation can better improve the tensile strength and the specified non-proportional extension strength of the alloys than the

hydrogen-free carbonization. Compared with that of the Original specimens, the elongation of the Ti-C-O specimens increases by 17.8%, and the reduction of area decreases by 7.1%. After the hydrogen-free carburization on the titanium surface, the elongation and the reduction of area decrease by 38%~56% and 27.6%~46.9%[5], respectively, compared with those of the Original specimen. It can be concluded that after the oxygen-carbon co-cementation, the overall performance of Ti6Al4V alloy is superior to that after hydrogen-free carburization. Therefore, the oxygen-carbon co-cementation has a greater influence on the mechanical properties of Ti6Al4V alloy, which are almost equivalent to those of the Original specimen. This result indicates that the oxygen-carbon co-cementation can maintain the mechanical properties of the Ti6Al4V alloy and simultaneously improve the hardness.

#### 2.5.2　Fracture appearance

Fig. 11 shows the fracture appearances of Ti6Al4V alloy specimens with and without oxygen-carbon co-cemented coating. It can be seen that the fracture length of oxygen-carbon co-cemented alloy specimen is significantly longer than that of the original specimen. The tensile fracture basically occurs in the middle part of the oxygen-carbon co-cemented specimen, and the obvious necking phenomenon can be observed, suggesting the plastic fracture. In the tensile fracture process, the co-cemented layer peels off continuously. The peeling starts at the middle part and gradually extends to the bottom area. After the specimen fractures, the specimen surface is full of pits with annular or intermittent annular cracks. The number of cracks is gradually increased from the bottom to the middle part of the specimen. The cracks at the bottom are small, and become wider towards the middle part. The cracks are mainly concentrated around the fracture area, and less cracks exist at the bottom area of the specimen.

#### 2.5.3　Co-cemented coating morphology

Fig. 12 shows SEM morphologies and EDS analysis results of Ti6Al4V alloy specimens with and without oxygen-carbon co-cemented coating. It can be seen from Fig. 12e that there are cracks on the surface of the oxygen-carbon co-cemented alloy specimen, which are annular or discontinuously annular. The obvious necking phenomenon occurs on the surface of oxygen-carbon co-cemented specimen, but not on the alloy surface with hydrogen-free carburized coating (Fig. 13).



| Element | Al | V | Ti |
| --- | --- | --- | --- |
| wt% | 5.69 | 4.08 | 90.23 |

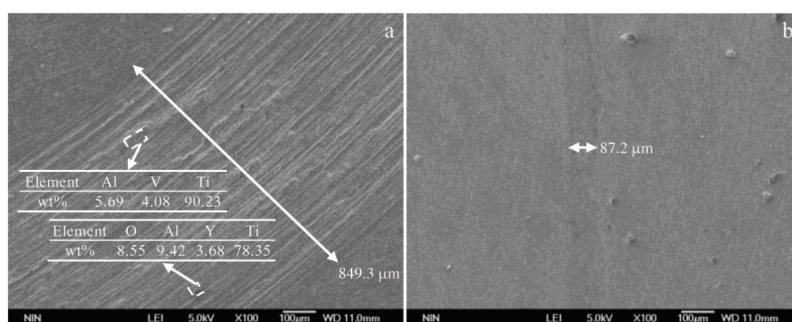| Element | O | Al | V | Ti |
| --- | --- | --- | --- | --- |
| wt% | 8.55 | 9.42 | 3.68 | 78.35 |

Fig.9　Wear morphologies and EDS results of Ti6Al4V alloys without (a) and with (b) oxygen-carbon co-cemented coating
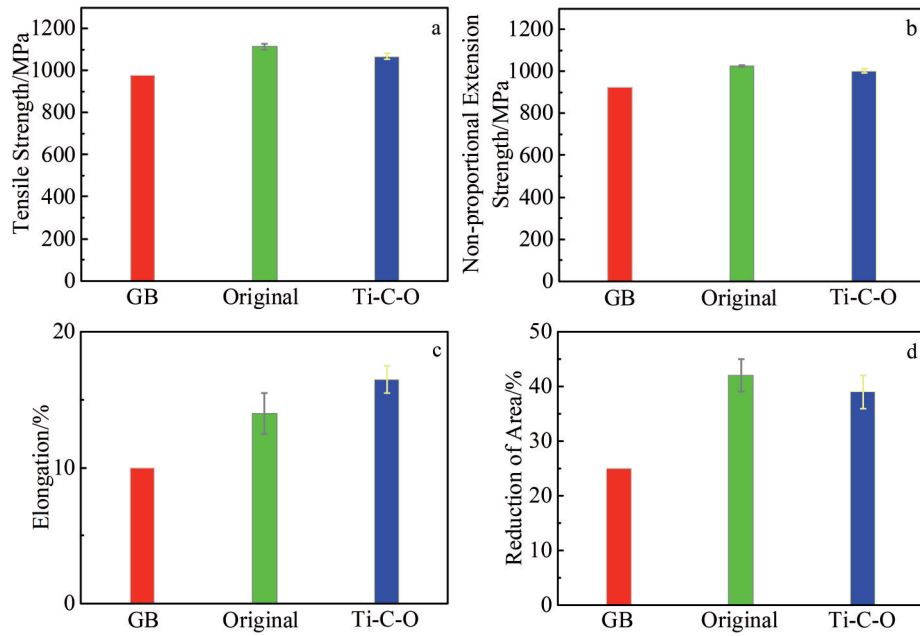
Fig.10    Tensile properties of GB, Original, and Ti-C-O specimens



Fig.11    Fracture appearances of Ti6Al4V alloy specimens with and without oxygen-carbon co-cemented coating

According to Fig. 12e, the Ti6Al4V alloy specimen with oxygen-carbon co-cemented coating shows obvious peeling phenomenon, and the dimples can be found at the fracture area. The ductile fracture characteristics of the coated specimen are similar to those of the specimen without coating. According to EDS analysis of the peeling area in Fig.12f, the composition is basically the same as that at Point 3 in Fig.5a, which indicates that the brittle area of the co-cemented layer
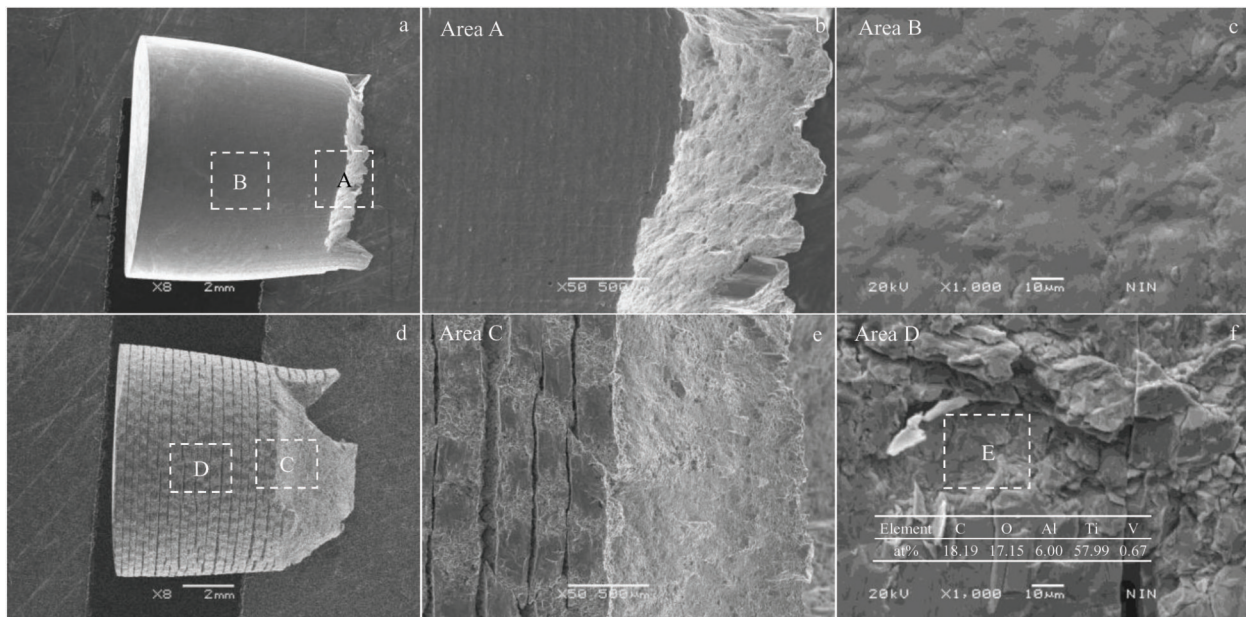


Fig.12    SEM morphologies of Ti6Al4V alloy specimens without (a~c) and with (d~f) oxygen-carbon co-cemented coating: (a, d) fracture appearance; (b, c, e, f) magnified image of area A, B, C, and D, respectively (EDS analysis result of area E is shown in Fig.12f)
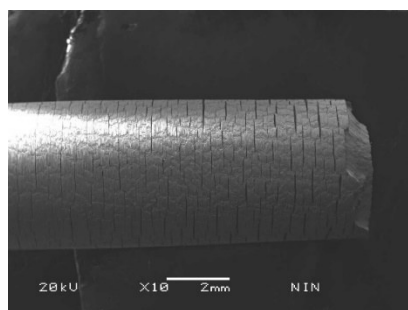
Fig.13    SEM morphology of Ti6Al4V alloy with hydrogen-free carburized coating[5]

mainly exists in the thin area of the surface, and the continuous cracks and peeling defects on the surface decrease the strength of the alloy specimen.

2.5.4    Tensile fracture morphology

Fig. 14 shows SEM fracture morphologies of the tensile specimens. It can be seen that the oxygen-carbon co-cemented specimen shows the plastic fracture characteristics, which are obviously different from those of the hydrogen-free carburized alloy[5]. Compared with the original specimen in Fig. 14a, the oxygen-carbon co-cemented specimen has a certain directionality, i. e., the pulling is along a certain direction, as indicated by the arrow in Fig.14b.
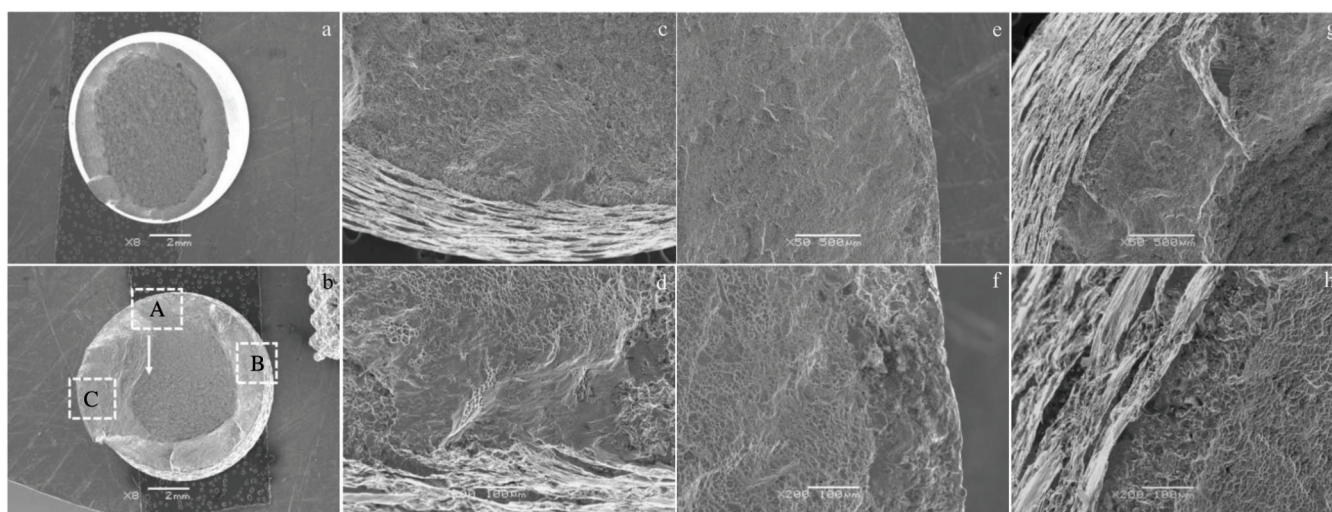


Fig.14    SEM fracture morphologies of Ti6Al4V alloy specimens without (a) and with (b~f) oxygen-carbon co-cemented coating: (c, d) magnified images of area A in Fig.14b; (e, f) magnified images of area B in Fig.14b; (g, h) magnified images of area C in Fig.14b

Fig. 14c and 14d exhibit the fracture source, which shows the plastic characteristic. After the oxygen-carbon co-cementation, the surface of the tensile specimen consists of a hard layer. During the tensile process, the layer peels off continuously, and the defects are formed on the tensile surface. As a result, the fracture sources appear at the defects under the three-dimensional stress.

The characteristics of the edges are similar in Fig.14e~14h, but they are quite different from the dimples in the inner area. Since the dimples represent the plastic deformation ability of the material, it can be concluded that the edge area has the characteristics of plastic ductile fracture.

## 3  Conclusions

1) The oxygen-carbon co-cementation changes the microstructure of Ti6Al4V alloy because of the appearance of TiC and $TiO_x$ phases.

2) The hardness of Ti6Al4V alloy is increased sharply after the oxygen-carbon co-cementation. The surface hardness is 13 014 MPa, which is 3.8 times higher than that of the substrate. The coating hardness changes gradually with the coating depth, and the carbon content can reflect the hardness change trend.

3) The wear resistance of Ti6Al4V alloy is significantly improved after the oxygen-carbon co-cementation: the friction state of the original Ti6Al4V alloy changes, only slight traces can be found on the surface, and no wear occurs. After the oxygen-carbon co-cementation, the wear rate and friction coefficient are about 3.5% and 30% of those of the original Ti6Al4V alloy, respectively.

4) During the tensile fracture process, the outer surface of the co-cemented layer peels off continuously, and thus the strength of the specimen slightly decreases. The reduction of area and the elongation are basically equivalent to those of the original Ti6Al4V alloy. The oxygen-carbon co-cemented Ti6Al4V alloy has the plastic fracture.

## References

1  Leyens C, Peters M. *Titanium and Titanium Alloys: Fundamentals and Applications*[M]. Weinheim: Wiley-VCH, 2003: 1

2  Lvtjering G, Williams J C. *Titanium*[M]. Berlin: Springer, 2007: 3

3  Ji Shouchang, Li Zhengxian, Du Jihong *et al. Rare Metal Materials and Engineering*[J], 2010, 39(12): 2152 (in Chinese)

4  Ji Shouchang, Li Zhengxian, Luo Xiaofeng *et al*. *Rare Metal Materials and Engineering*[J], 2014, 43(12): 3114 (in Chinese)

5  Ji Shouchang, Li Zhengxian, Wang Yanfeng *et al*. *Rare Metal Materials and Engineering*[J], 2016, 45(10): 2734 (in Chinese)

6  Ji Shouchang, Li Zhengxian, Chang Chenyang *et al*. *Titanium Industry Progress*[J], 2017, 34(6): 20 (in Chinese)

7  Zhao Yun, Zhang Yulin, Zeng Yun *et al*. *Rare Metal Materials and Engineering*[J], 2017, 46(6): 1503

8  Zabler S. *Materials Characterization*[J], 2011, 62(12): 1205

9  Zhang Yang, Ma Guorong, Zhang Xiancheng *et al*. *Corrosion Science*[J], 2017, 122(1): 61

10 Ma Hongyan, Wang Maocai, Wei Zheng. *Rare Metal Materials and Engineering*[J], 2007, 36(4): 685 (in Chinese)

11 Luo Yong, Chen Wenwen, Tian Maocai *et al*. *Tribology International*[J], 2015, 89: 67

12 Grotberg J, Hamlekhan A, Butt A *et al*. *Materials Science and Engineering C*[J], 2016, 59: 677

13 Cao L, Liu J, Wan Y *et al*. *Surface and Coatings Technology*[J], 2018, 337: 471

14 Song M H, Han S M, Min D J *et al*. *Scripta Materialia*[J], 2008, 59(6): 623

15 Ma Hongyan, Wang Maocai, Wu Weitao. *Journal of Materials Science and Technology*[J], 2004, 20(6): 719

16 Jiang Yong, Mao Hairong, Wang Xiaowei *et al*. *Surfaces and Interfaces*[J], 2021, 25: 101 248

17 Yan Wei, Wang Xiaoxiang. *Rare Metal Materials and Engineering*[J], 2005, 34(3): 471 (in Chinese)

18 Li Zhengxian, Du Jihong, Ji Shouchang *et al*. *China Patent*, 200710188530.3[P], 2009 (in Chinese)

19 Wang Haonan, Li Zhengxian, Zhao Wen *et al*. *China Patent*, 201611091389.0[P], 2018 (in Chinese)

20 Li Zhengxian, Ji Shouchang, Du Jihong *et al*. *China Patent*, 201210199053.1[P], 2014 (in Chinese)

21 Ji Shouchang, Li Zhengxian, Du Jihong *et al*. *China Patent*, 202210576891.X[P], 2022 (in Chinese)

22 Menzies I A, Strafford K N. *Journal of the Less Common Metals*[J], 1967, 12(2): 85

23 Menzies I A, Strafford K N. *Corrosion Science*[J], 1975, 15(2): 69

24 Menzies I A, Strafford K N. *Corrosion Science*[J], 1975, 15(2): 91

25 Kusabiraki K, Kuroda N, Motohira I *et al*. *Oxidation of Metals*[J], 1997, 48(3): 289

26 Aresta M, Dibenedetto A, Quaranta E. *Reaction Mechanisms in Carbon Dioxide Conversion*[M]. Berling: Springer, 2016

27 Jeung G H. *Molecular Physics*[J], 1989, 67(4): 747

# 钛合金氧碳共渗层性能

姬寿长 [1,2,3]，李京龙 [1,2]，王少鹏 [3]，杨海彧 [3]，畅晨阳 [3]
(1. 西北工业大学 凝固技术国家重点实验室，陕西 西安 710072)
(2. 西北工业大学 陕西省摩擦焊接工程技术重点实验室，陕西 西安 710072)
(3. 西北有色金属研究院，陕西 西安 710016)

摘　要：将经磨平、抛光、超声波乙醇清洗、吹干的 Ti6Al4V 合金样品放入专用设备中进行氧碳共渗。分别采用 X 射线衍射仪（XRD）、扫描电子显微镜（SEM）、能谱仪（EDS）、HV 硬度仪、万能材料试验机对渗层的物相、显微组织形貌、成分、硬度、摩擦磨损、力学性能进行分析。XRD 结果表明，渗层中出现 TiC 和 $TiO_x$ 相。氧碳共渗改变了原 Ti6Al4V 合金的组织，渗层的显微组织明显区别于 Ti6Al4V 的渗碳、渗氧以及在 $CO_2$ 气氛下处理的组织。EDS 结果表明，C、O 元素含量呈现梯度变化。相比基体硬度，渗层表面硬度提高了 3.8 倍，渗层硬度呈梯度变化。氧碳共渗改变了原始样的粘着磨损和摩擦状态，渗层样表面只有轻微的摩擦痕迹、无磨损。氧碳共渗后磨损量是原始样的 3.5%，摩擦系数约为原始样的 30%。渗层样在拉断过程中，外表面有一定的剥落，表面布满裂纹，样品的强度略有下降，断面延伸率和断面收缩率与原始样相当。Ti6Al4V 合金经过氧碳共渗后，提高了表面硬度，降低了磨损率和摩擦系数，基本保持了基体的力学性能。

关键词：钛；氧碳共渗；硬度；耐磨性能；力学性能

作者简介：姬寿长，男，1981 年生，博士生，教授，西北有色金属研究院，陕西 西安 710072，电话：029-86283410，E-mail：jscnin@163.com